How to Cite: Tazhbayev, Y.M., Galiyeva, A.R., Syrymova, U.Y., Zhaparova, L.Zh., & Zhumagaliyeva, T.S. (2026). Rifampicin Loaded Chitosan-Based Nanoparticles: Optimization, Characterization, and Mucoadhesion. *Eurasian Journal of Chemistry, 31, 1(121), 45–60.* https://doi.org/10.31489/2959-0663/1-26-4

Article

Received: 28 November 2025 | Revised: 27 February 2026 | Accepted: 3 March 2026 | Published online: 13 March 2026

UDC 541.64

https://doi.org/10.31489/2959-0663/1-26-4

Yerkeblan M. Tazhbayev, Aldana R. Galiyeva *, Ulpan Y. Syrymova, Lyazzat Zh. Zhaparova, Tolkyn S. Zhumagaliyeva

Karaganda National Research University named after Academician Ye.A. Buketov, Karaganda, Kazakhstan
*(*Corresponding author's e-mail: aldana_karaganda@mail.ru)*

Rifampicin Loaded Chitosan-Based Nanoparticles: Optimization, Characterization, and Mucoadhesion

One of the important problems in modern pharmaceutical technology is the development of effective and safe drug delivery systems. In this regard, the development of nanostructures that deliver drugs in a targeted manner and increase their bioavailability is of particular importance. Biodegradable polymers form the basis of such systems. Among natural polysaccharides, chitosan deserves special attention. Colloidal particles made from chitosan, especially nanoparticle-based systems, increase the solubility of drugs and enable their effective delivery through the mucosal layer. This study aimed to prepare chitosan nanoparticles loaded with an anti-tuberculosis drug (rifampicin) using the ionotropic gelation method. A central composite design (CCD) was used to study the effects of chitosan concentration, rifampicin concentration, medium pH, and ethanol volume on particle size, polydispersity, and nanoparticle yield. The optimized nanoparticles were spherical in shape with an average particle size of 386±9 nm and a polydispersity index of 0.259±0.025. The rifampicin loading and nanoparticle yield of the optimized nanoparticles were 20 % and 71 %, respectively. The produced nanoparticles were analyzed using thermogravimetric analysis (TGA) and differential scanning calorimetry (DSC), and the results showed no interaction between the drug and the polymer. Drug release from the polymer matrix was studied at different pH values stimulating the gastrointestinal tract. The mucoadhesive activity of rifampicin-loaded chitosan nanoparticles was investigated through the interaction with mucin in acetate buffer solution (pH 5.5) and phosphate buffer solution (pH 6.8). The results showed higher mucoadhesive activity in an acetate buffer solution.

Keywords: drug delivery, rifampicin, bioavailability, nanoparticles, chitosan, tuberculosis, anti-tuberculosis drugs, ionic gelation, mucoadhesion, mucin

Introduction

Tuberculosis represents a significant threat to global health, ranking as the second leading cause of death from infectious diseases after human immunodeficiency virus (HIV). Approximately 10 million people worldwide are diagnosed with tuberculosis annually, and this figure has been increasing since 2020 [1]. Among several anti-tuberculosis drugs, rifampicin (RIF) is considered one of the most effective and plays an important role in short-term therapy. Rifampicin is a model anti-tuberculosis drug with good chemical and physical properties. However, it also has limitations, such as low bioavailability, drug resistance, low permeability through cell membranes, insufficient access to the infected areas, and degradation before reaching its destination [2]. Therefore, it is advisable to develop an alternative delivery system for rifampicin and a method for its implementation. The situation is complicated by the fact that each year more than 15 % of patients are found to have multiple drug resistance or resistance to rifampicin [3] due to non-compliance with the dosage regimen by the patient. The use of natural polymer carriers is a promising solution to these problems. Delivering drugs using nanoscale carriers can increase their bioavailability and significantly prolong the effect of the drug. This is especially important when resistance to anti-tuberculosis drugs develops.

Previously, several polymers were used to manufacture nanoparticles for delivery through the lungs, including polylactide, polylactide-co-glycolide, albumin, chitosan, and alginates [3–6]. The natural polymer chitosan, containing β-(1 → 4)-linked D-glucosamine and N-acetyl-D-glucosamine, is widely used due to its biological solubility, biocompatibility, ability to bind to the mucous membrane (depending on the positive charge in an aqueous environment), low toxicity, and antimicrobial activity [7–10]. In addition, chitosan has high adhesion, enabling it to bind effectively with alveolar macrophages and helps achieve the goal.

Colloidal particles made from chitosan, especially in the form of nanoparticles, increase the solubility of drugs and enable their effective delivery through the mucous layer [11–13]. The large surface area of col-

© 2026 The Authors. This is an open access article under the CC BY-NC-ND license (http://creativecommons.org/licenses/by-nc-nd/4.0/)

loidal particles and their special physicochemical properties allow them to be used as carriers for drugs, adsorbents, and biomaterials [14, 15]. However, the process of producing chitosan colloidal particles depends on a number of factors and requires certain conditions. The correct selection of parameters for this process directly affects the properties (size, shape and stability) of the resulting particles. Modern mathematical and statistical methods are used to determine the optimal conditions. One of them is the central composite design (CCD) method. This method allows describing multifactorial systems, determining the relationship between variables, and developing a mathematical model. Its advantage is that it allows obtaining extensive data from a limited number of experiments, which saves time and resources.

In this work, the process was optimized using the central composite design method to produce rifampicin-loaded chitosan colloidal particles (CS-RIF) by a modified ionotropic gelation method. Although rifampicin-loaded chitosan nanoparticles have previously been obtained using ionotropic gelation and optimized using statistical design methods, limitations related to the low solubility of rifampicin and poor control over nanoparticle size and loading efficiency remain insufficiently addressed. In this study, ethanol is introduced as an additional formulation factor in a modified ionotropic gelation process and systematically optimized using a central composite design. The inclusion of ethanol improves the solubility of rifampicin and promotes the formation of nanoparticles with reduced size and a narrower size distribution. Chitosan concentration, rifampicin concentration, pH of the medium, and ethanol volume were selected as factors influencing the particle size and polydispersity index (PDI) of the CS-RIF nanoparticles. The aim of this study is to develop rifampicin-loaded chitosan nanoparticles and to investigate their physicochemical characteristics, drug release kinetics, and mucoadhesive properties.

Experimental

Materials

The following reagents were used in the experiment: low molecular-weight chitosan, rifampicin, sodium tripolyphosphate (TPP), Sodium Acetate Anhydrous (>99 %) and porcine gastric mucin Type II from Sigma-Aldrich (Germany), ethanol 90 % (Dosfarm, Kazakhstan) and acetic acid (Scat Company, Kazakhstan).

Purification of Chitosan

To purify chitosan, we used the method reported by Yang et al [16]. For this purpose, 0.3 g of chitosan was weighed and stirred until completely dissolved in 30 mL of 0.1 M hydrochloric acid (HCl) solution. The solution was continuously stirred in an orbital shaker-incubator at 40 °C overnight. Then the solution was filtered and centrifuged at 10,000 g for 1 hour, and the supernatant was collected. 0.5 M NaOH solution was added dropwise to the supernatant until the pH was reached 10 and a white precipitate appeared. The mixture was centrifuged at 5,000 g for 30 minutes. The supernatant was removed, and the chitosan precipitate remained at the bottom of the tubes. Distilled water was added to the tubes, and the mixture was centrifuged at 5,000 g for 10 minutes. The chitosan precipitate was placed in a Petri dish and dried by lyophilization for 4-5 hours.

Preparation of CS-RIF Nanoparticles

Nanoparticles based on chitosan and rifampicin were synthesized using the ionotropic gelation method with some modifications [17, 18]. Purified chitosan (0.4 g) was dissolved in 0.05 % acetic acid (40 mL) and continuously stirred in an orbital shaker-incubator at 40 °C overnight. The resulting chitosan solution was adjusted to the required pH (4, 5 or 6). The chitosan solution was mixed with deionized water to produce a CS solution with a concentration of 2.5, 5 or 7.5 mg/mL. Rifampicin was dissolved in a 0.15 % DMSO solution to obtain a concentration of 0.25, 0.5 or 0.75 mg/ mL. The resulting drug solution was added to the CS solution and stirred for 10 minutes. To the CS-RIF solution, 4, 6 or 8 mL of 90 % ethanol was added dropwise at a rate of 1 mL/min. Finally, 0.5 % sodium tripolyphosphate (TPP) was added dropwise at a CS:TPP ratio of 3:1, and the resulting mixture was stirred at room temperature for 6 hours. Next, the nanoparticles were separated using a centrifuge (Eppendorf 5420, Hamburg, Germany) at 15,000 rpm for 30 minutes. The nanoparticles were purified with distilled water three times by centrifugation. A schematic representation of the method for producing nanoparticles is shown in Figure 1.

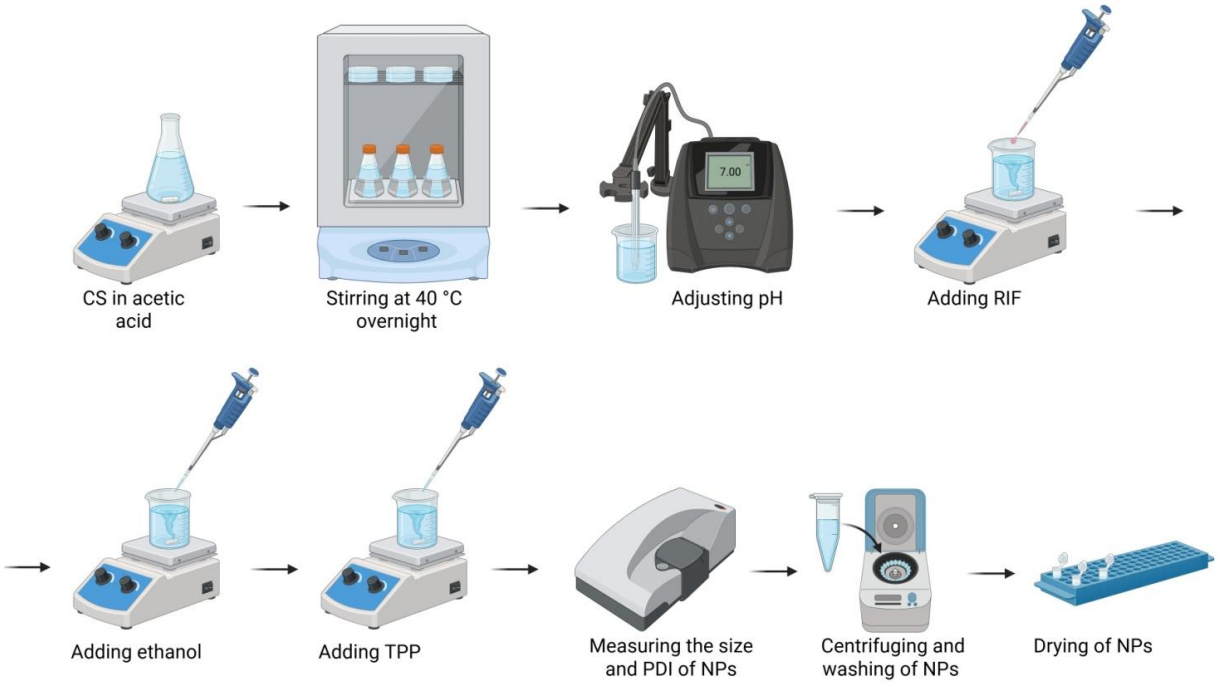

Illustration created in BioRender. Galiyeva, A. (2026) https://BioRender.com/ieb2gof

Figure 1. Schematic illustration of production CS-RIF nanoparticles by ionic gelation method

Central Composite Design for Nanoparticle Optimization

Optimization of CS-RIF nanoparticle production was performed using a central composite design with various factors, including chitosan concentration, rifampicin concentration, medium pH, and ethanol content. Design Expert® software (version 13, Stat-Ease, Minneapolis, Minnesota, USA) was used to create a CCD matrix of four factors with three levels each (Table 1).

Table 1

Experimental factors for CS-RIF nanoparticle synthesis and corresponding levels

Independent Variable	Variable Level		
	Low –1	Center 0	High 1
Concentration of CS, mg/mL	2.5	5	7.5
Concentration of RIF, mg/mL	0.25	0.5	0.75
pH	4	5	6
Ethanol volume, mL	4	6	8

Determination of Particle Size, Polydispersity and ζ-potential of CS-RIF nanoparticles

The nanoparticle size distribution and polydispersity index were measured using Zetasizer Nano S90 (Malvern Instruments Ltd., Malvern, UK) by Dynamic Light Scattering (DLS). For the size analysis of CS-RIF nanoparticles, 5–8 drops of nanoparticles suspension were added to 1.5–2 mL of distilled water. The measurements of the samples were conducted at 25 °C while using a 90° scattering angle for detection.

Evaluation of Drug Loading Efficiency and Nanoparticles' Yield

For spectrophotometric measurements of nanoparticle solutions loaded with a drug substance, RIF solutions were prepared at various concentrations as reference values. Measurements were performed using a UV spectrophotometer (Shimadzu UV-1800 dual-beam scanning spectrophotometer, Japan). The absorbance of the samples was measured at a wavelength of 470 nm (λ) against a 0.15 % DMSO solution.

To determine the yield, the nanoparticles were left to dry for several days and their mass was measured. The loading efficiency of drug and nanoparticles yield were calculated using the following formulas:

$$\text{Loading efficiency}\left(LE,\,\%\right)=\frac{\text{Total mass of } RIF-\text{mass of free } RIF}{\text{Mass of } NPs}\times 100\ \%$$

$$\text{Nanoparticles yield}\left(\%\right)=\frac{\text{Mass of } NPs}{\text{Total mass of } RIF+\text{mass of } CS+\text{mass of } TPP}\times 100\ \%$$

In Vitro Drug Release from CS-RIF nanoparticles

The kinetics of rifampicin release from the polymer matrix were determined by the dialysis dilute HCl or in phosphate-saline buffer at 37 °C in three different environments (0.2 M HCl with pH 1.2, 0.1 M phosphate buffer with pH 6.8 and 7.4). For this purpose, 24 mg drug-loaded nanoparticles were dispersed in 3 mL phosphate buffer and treated with ultrasound for 10 minutes. The resulting dispersion was transferred to a dialysis membrane (MwCO: 8,000–14,000 D). The membrane was fixed on both sides with clamps, placed in a container with 14 mL dilute HCl or phosphate-saline buffer and placed in a thermostat at 37 °C. The amount of drug released from the polymer nanoparticles was determined by UV spectroscopy (wavelength λ = 470 nm), and the degree of release was calculated using the following formula:

$$\text{Drug release }\left(\%\right)=\frac{\text{Mass of released } RIF}{\text{Mass of total } RIF \text{ in nanoparticles}}\times 100\ \%$$

Thermogravimetry and Differential Scanning Calorimetry Analysis of CS-RIF nanoparticles

Thermogravimetric and differential scanning calorimetric studies were performed using a LabSYS evo TGA/DTA/DSC analyzer (Setaram, Caluire, France). Measurements were performed in the temperature range from 30 °C to 915 °C. The samples were placed in aluminium oxide crucibles and heated at a controlled rate of 10 °C/min. The analysis was carried out in a nitrogen atmosphere at a constant gas flow rate of 30 mL/min.

Infrared Spectroscopic Analysis of CS-RIF nanoparticles

The characteristics of the produced nanoparticles and rifampicin samples were studied using IR spectroscopy with an FSM 1202 spectrometer (Infraspek Ltd., Russia). The potassium bromide pellet method was used to record Fourier transform infrared (FTIR) spectra. The spectra were recorded in the wavenumber range from 4000 to 400 cm^{-1}.

Study of the Mucoadhesive Properties of CS-RIF Nanoparticles

To study the mucoadhesive properties, the turbidimetric method with a Hach 21000AN laboratory turbidimeter (Hach Company, USA) was used [19–21]. To assess the effect of the medium on the mucoadhesive properties, two different buffer solutions were used: an acetate buffer solution (pH 5.5) and a phosphate buffer solution (pH 6.8). In each buffer medium, 0.0015 g of mucin was dissolved and the initial optical density was measured at 255 nm. Then 0.0195 g of rifampicin-loaded chitosan nanoparticles were added to the same solution. The solution was incubated at 37 °C and the optical density was measured for 4 hours to study the dynamics of the mucoadhesive effect. The interaction of mucin with CS-RIF nanoparticles was calculated using the following equation:

$$\text{Mucin binding efficiency}\left(\%\right)=\frac{\text{Absorbance}_{\text{sample}}-\text{Absorbance}_{\text{initial}}}{\text{Absorbance}_{\text{sample}}}\times 100\ \%.$$

Statistical Analysis

All experiments were carried out at least three times. The results are reported as means with standard deviations. To analyze independent groups, a one-way analysis of variance was applied using Minitab19 software. The effect of the suggested experiments on the responses was analyzed using Design Expert software to generate the main effects of various factors regardless of each other, and then an analysis of variance (ANOVA) was performed to determine statistically significant factors. The optimal experimental conditions were identified by selecting the function.

Results and Discussion

There are various methods for producing chitosan-based nanoparticles, including ionotropic gelation, nanoparticle deposition, and emulsification-based methods [22–26]. Among them, ionotropic gelation is one

of the most commonly used methods due to the use of mild reagents, a simple preparation process, and ease of controlling the size of the nanoparticles. In this method, ionic mixing occurs between the protonated amino groups of chitosan and the negatively charged groups of polyanion (sodium tripolyphosphate), thus forming nanoparticles [27]. Using a previously developed technique [17, 18], chitosan nanoparticles loaded with rifampicin were produced at the initial stage. The particle size of CS-RIF NPs and their polydispersity are not good enough (diameter more than 823±11 nm, PDI 0.742±0.049), which limits their potential use as drug delivery systems in the body. Thus, it is necessary to optimize the method specifically for producing chitosan-rifampicin nanoparticles, taking into account the properties and solubility of the active substance. The novelty of this work is the addition of ethanol during the production of CS-RIF nanoparticles. Ethanol plays several roles in the creation of nanoparticles by ionotropic gelation method. Ethanol increases the solubility of rifampicin, thereby improving the drug loading efficiency in the polymer matrix. It also reduces interfacial tension in particle-particle interactions, thus preventing nanoparticle aggregation [28–30]. Therefore, ethanol acts not only as a co-solvent, but also as a key factor in regulating nanoparticle size and drug loading efficiency.

The aim of this study is to optimize the parameters for producing rifampicin-loaded chitosan-based nanoparticles. To achieve this goal, key factors such as chitosan concentration, rifampicin concentration, medium pH and ethanol volume were analyzed. In addition, the physicochemical properties, drug release from the polymer matrix at different pH values, and mucoadhesive properties of the produced CS-RIF nanoparticles were studied.

The central composite design method was used to optimize the above parameters. This optimization method allows the interactions of a large number of variables to be determined by conducting a limited number of experiments. Previously, the CCD method has demonstrated good results in optimizing the synthesis of nanoparticles for the delivery of antituberculosis drugs [3, 31]. To optimize the parameters of CS-RIF nanoparticles, 17 experiments were conducted. Table 2 shows the structure of the orthogonal matrix and the results of measuring the size and polydispersity of the particles, as well as the rifampicin loading efficiency and nanoparticle yield.

Table 2

Formulations of CS-RIF nanoparticles using central composite design and their evaluation parameters

Nanoparticles	[CS], mg/mL	[RIF], mg/mL	pH	Ethanol volume, mL	Size, nm	PDI	LE, %	NPs yield, %
NP 1	5	0.5	5	4	426±8	0.264±0.024	33±9	88±8
NP 2	7.5	0.75	4	4	563±4	0.751±0.122	38±8	20±4
NP 3	2.5	0.75	6	8	461±10	0.226±0.004	49±2	12±7
NP 4	5	0.75	5	6	427±9	0.247±0.014	36±8	94±9
NP 5	2.5	0.75	4	8	575±9	0.236±0.022	41±3	6±4
NP 6	5	0.5	5	6	491±13	0.233±0.030	20±8	28±3
NP 7	5	0.5	4	6	507±5	0.275±0.039	29±2	5±5
NP 8	7.5	0.25	4	8	528±7	0.527±0.049	36±2	4±2
NP 9	2.5	0.5	5	6	376±6	0.242±0.021	31±8	90±6
NP 10	7.5	0.25	6	8	315±9	0.307±0.137	37±4	54±6
NP 11	5	0.5	5	8	493±13	0.257±0.016	15±4	68±1
NP 12	2.5	0.25	6	4	347±2	0.264±0.004	40±8	17±4
NP 13	7.5	0.5	5	6	238±5	0.233±0.028	28±3	54±3
NP 14	2.5	0.25	4	4	425±8	0.364±0.061	38±8	11±3
NP 15	5	0.25	5	6	440±8	0.258±0.011	27±2	75±1
NP 16	7.5	0.75	6	4	371±15	0.434±0.262	45±2	93±8
NP 17	5	0.5	6	6	664±6	0.317±0.048	35±6	91±5

Results are shown as mean ± standard deviation (n = 3)

According to the results obtained (Table 2), depending on the synthesis conditions, CS-RIF nanoparticles with diameters ranging from 238±5 to 664±6 nm can be produced, with polydispersity also varying significantly from 0.226±0.004 to 0.751±0.122. The smallest particle size was in sample NP13 (238±5 nm) with a chitosan concentration of 7.5 mg/mL, rifampicin concentration of 0.5 mg/mL, pH of 5, and ethanol volume of 6 mL. The drug loading and nanoparticle yield values are also significant parameters, ranging from 15±4 % to 49±2 % and from 4±2 % to 93±8 %, respectively.

To determine the applicability and significance of the mathematical model for evaluating particle size, polydispersity, and NP yield, the analysis of variance (ANOVA) was used (Table 3).

Table 3

ANOVA results for particle size, polydispersity, and low-frequency yield

Response	Source	Sum of Squares	Degree of Freedom	Mean Square	F-value	p-value
Size	Model	27906.25	3	9302.08	0.8261	0.5027
	A — Concentration of CS	2859.48	1	2859.48	0.2539	0.6228
	B — Concentration of RIF	11710.08	1	11710.08	1.04	0.3272
	C — pH	19377.60	1	19377.60	1.72	0.2123
	D — Ethanol volume	5669.16	1	5669.16	0.5034	0.4905
	Residual	1.464E+05	13	11260.77		
	Cor Total	1.743E+05	16			
PDI	Model	0.1487	3	0.0496	4.20	0.0278
	A — Concentration of CS	0.0846	1	0.0846	7.16	0.0190
	B — Concentration of RIF	0.0030	1	0.0030	0.2413	0.6321
	C — pH	0.0366	1	0.0366	3.10	0.1019
	D — Ethanol volume	0.0275	1	0.0275	2.32	0.1513
	Residual	0.1536	13	0.0118		
	Cor Total	0.3023	16			
NPs yield	Model	6476.16	3	2158.72	1.93	0.1740
	A — Concentration of CS	792.10	1	792.10	0.7096	0.4148
	B — Concentration of RIF	432.96	1	432.96	0.3690	0.5549
	C — pH	4946.18	1	4946.18	4.43	0.0553
	D — Ethanol volume	737.88	1	737.88	0.6610	0.4308
	Residual	14511.93	13	1116.30		
	Cor Total	20988.08	16			

The ANOVA results showed that the size of the nanoparticles did not significantly depend on the investigated factors, indicating a possible influence of nonlinear effects or interactions. At the same time, the PDI index significantly depended on the chitosan concentration ($p = 0.0190$), confirming its key role in the formation of homogeneous particles. The model was statistically non-significant for nanoparticle yield, but pH showed a near-significant to significant effect ($p = 0.0553$), indicating its potential importance for further optimization. For PDI, the predicted R^2 value meaning which was equal to 0.0325, is not in reasonable agreement with the adjusted R^2 value (0.3747) and a similar discrepancy is observed for nanoparticles yield, where the predicted R^2 of 0.1108 is not as close to the adjusted R^2 of 0.4643. Nevertheless, the Adequate Precision for both responses (for PDI 7.8 and for nanoparticles yield 5.9) indicates an adequate signal and this model can be used to navigate the design space.

The model developed based on CCD for evaluating particle size, polydispersity and NP yield is presented below. In these formulas: A is the chitosan concentration, B is the rifampicin concentration, C is the pH, and D is ethanol.

$$\text{Size} = +449.94 - 16.91A + 34.22B - 44.02C + 23.81D$$

$$\text{PDI} = +0.3197 + 0.0920A + 0.0174B - 0.0605C - 0.0524D$$

$$\textbf{NPs yield} = +48.05 + 8.90A + 6.58B + 22.24C - 8.59D$$

The resulting regression equations showed that the size of nanoparticles depends most on pH, while polydispersity increases with increasing chitosan concentration and decreases with pH optimization and ethanol addition. The yield of nanoparticles is determined mainly by the pH value and, to a lesser extent, by the chitosan concentration. Thus, regulating the acidity of the medium is a key factor both for controlling particle size and uniformity as well as increasing their yield.

The influence of various factors on nanoparticle size, polydispersity, and NP yield is illustrated using a three-dimensional (3D) diagram (Figures 2–4).

Three-dimensional response diagrams show the influence of independent factors on the average size of nanoparticles (Figure 2). On the surface reflecting the combined effect of chitosan and rifampicin concentra-

tions, it can be seen that changes in these parameters have virtually no significant effect on particle size. These graphs are consistent with the results of the analysis of variance (ANOVA), where these factors did not show statistical significance. In contrast, the diagram in Figure 2*b*, reflecting the influence of pH and ethanol volume, shows more pronounced dynamics. With an increase in pH, there is a tendency for particle size to decrease, which is explained by a reduction in the degree of protonation of chitosan amino groups and, as a result, a decrease in electrostatic repulsion between polymer chains and a reduction in their degree of hydration [32]. Analysis of the response surface shows a slight increase in the size of chitosan nanoparticles at higher ethanol volumes (from 426 to 473 nm), although the ANOVA results ($p = 0.4905$) indicate low statistical significance. This suggests that ethanol is not a major independent factor. But it may indirectly influence nanoparticle formation by altering the polarity of the medium and modulating the effect of pH or chitosan concentration.

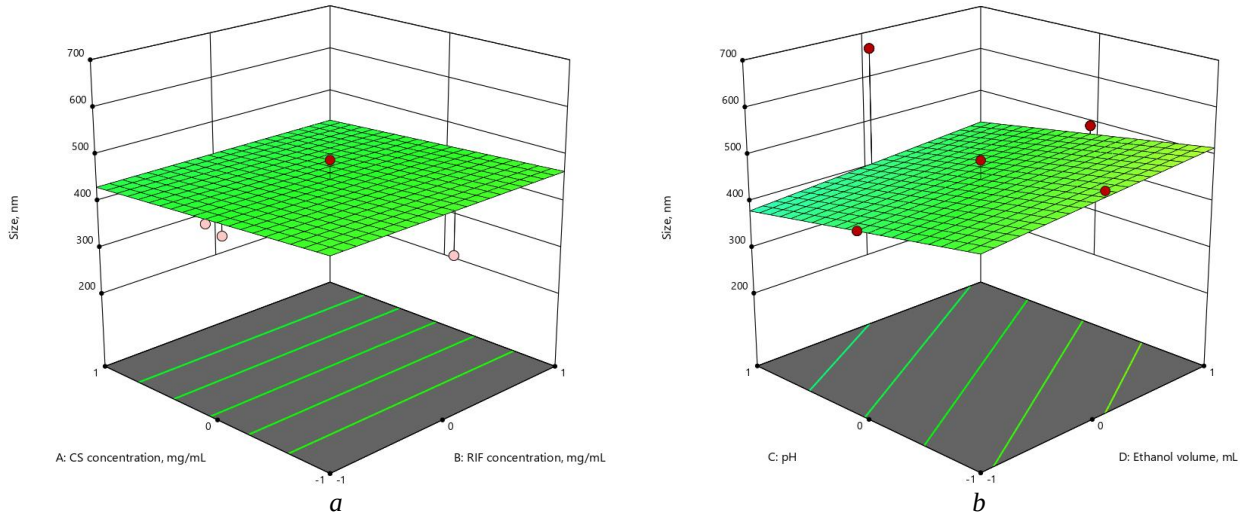

Figure 2. Three-dimensional (3D) response surface diagrams of the impact of independent factors on average particle size: (*a*) CS concentration – RIF concentration; (*b*) pH – Ethanol volume

Figure 3 shows 3D diagrams of the influence of independent variables on the polydispersity of the obtained particles. Graph 3a shows that chitosan concentration has a significant influence on PDI, as mentioned in the ANOVA analysis. As the chitosan concentration increases, the polydispersity increases from 0.228 to 0.406.

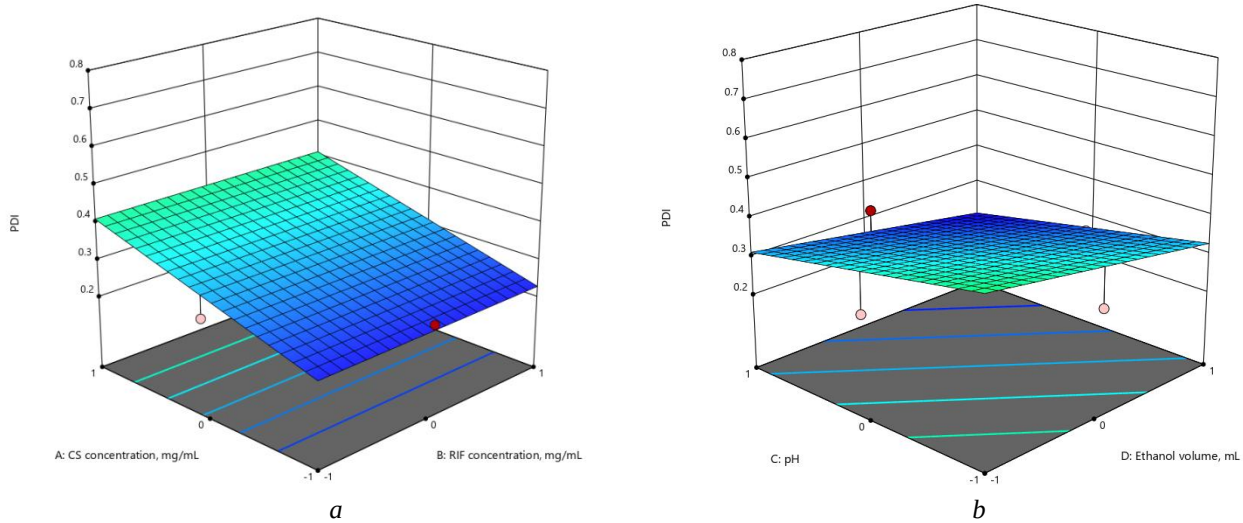

Figure 3. Three-dimensional (3D) response surface diagrams of the impact of independent factors on PDI: (*a*) CS concentration – RIF concentration; (*b*) pH – Ethanol volume

The response surface diagrams in Figure 4 show that the yield of nanoparticles increases at high pH, while an increase in ethanol volume leads to a decrease in yield. This dependence is explained by a decrease in the solubility of chitosan and partial destabilization of the ionic cross-linking process in the presence of ethanol. Although the model is not statistically significant (p = 0.174), the observed trend indicates that maintaining a moderate pH value and minimum ethanol content promotes more efficient nanoparticle formation.

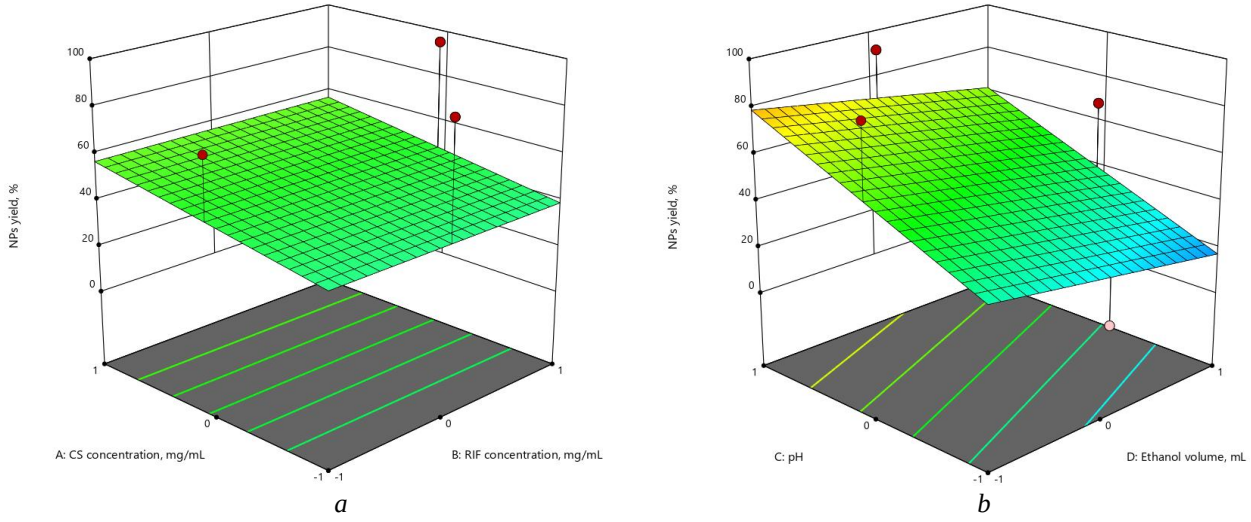

Figure 4. Three-dimensional (3D) response surface diagrams of the impact of independent factors on nanoparticles yield: (*a*) CS concentration – RIF concentration; (*b*) pH – Ethanol volume

After ANOVA analysis, parameters for computer optimization were selected using the Design Expert program. Table 4 shows the criteria used for optimization to obtain CS-RIF nanoparticles with minimum size and maximum yield.

Table 4

Limitations on independent variables and outcomes for optimization production CS-RIF nanoparticles

Name	Goal	Lower Limit	Upper Limit
A: CS concentration	is in range	–1	1
B: RIF concentration	is equal to 0	–1	1
C: pH	is equal to 1	–1	1
D: Ethanol volume	is in range	–1	1
Size	minimize	238.2	663.8
PDI	minimize	0.226	0.751
NPs yield	maximize	4	94.9

The program suggested the following parameters as optimal conditions: chitosan concentration 3.7 mg/mL, rifampicin concentration 0.46 mg/mL, ethanol volume 4 mL, pH value 6.0. Thus, using the recommended program parameters, rifampicin-loaded nanoparticles were synthesized. The characteristics of the produced chitosan nanoparticles were close to the values suggested by the program (Table 5). Consequently, the CCD method is effective for optimizing the synthesis process of CS-RIF nanoparticles (Figure 5).

Table 5

Predicted and experimental results for CS-RIF nanoparticles

	Size, nm	PDI	Yield, %
Predicted	390±10	0.264±0.108	74±3
Experimental	386±9	0.259±0.025	71±2
Error (%)	1	1.9	3.8
All values represent the mean ± S.D. (n = 3)			

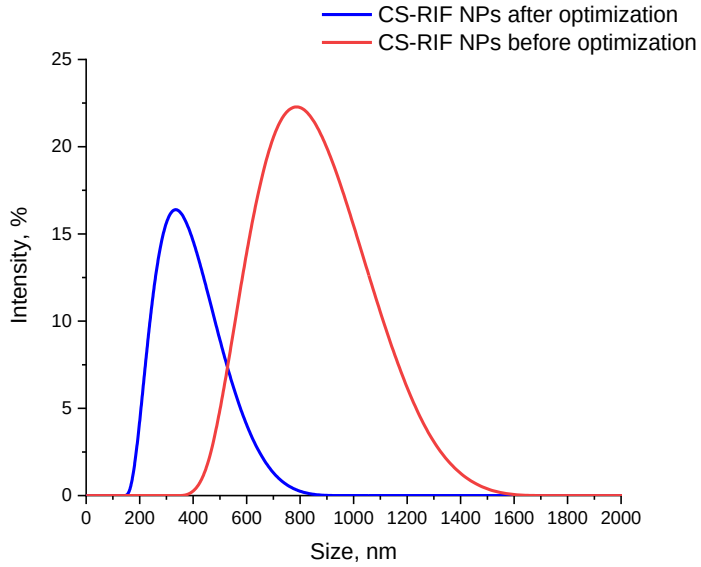

Figure 5. Size distributions of CS-RIF nanoparticles measured by DLS before and after optimization

In order to determine the morphology of nanoparticles obtained under optimal conditions without drugs (CS NPs) and rifampicin-loaded nanoparticles (CS-RIF NPs), scanning electron microscopy (SEM) images were acquired (Figure 6). The images show that the particles are predominantly spherical in shape and relatively homogeneous.

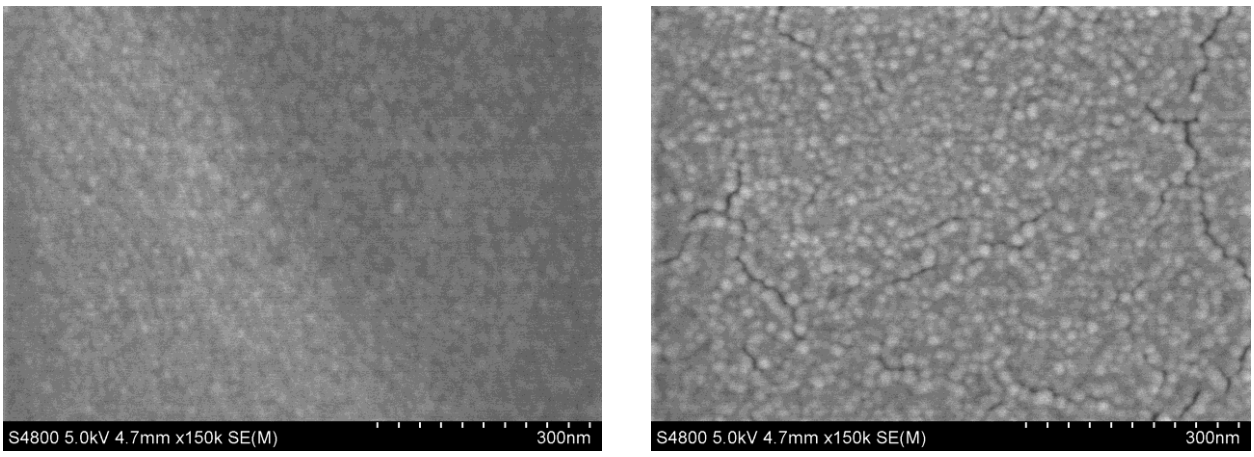

CS NPs CS-RIF NPs

Figure 6. SEM images of CS nanoparticles and CS-RIF nanoparticles at a 300 nm scale

The TGA and DSC results for pure chitosan, rifampicin, and nanoparticles are shown in Figure 7. The first stage of chitosan weight loss (Figure 7*a*) was observed in the temperature range of 40–100 °C, which corresponds to moisture loss (about 10 %). Under a nitrogen flow, chitosan undergoes thermal decomposition in the temperature range from 150 to 600 °C, which indicates chitosan deacetylation, the evaporation, and removal of volatile products [33, 34]. The DSC thermogram of chitosan showed an endothermic peak at 226 °C, which reflects the initial decomposition, and an exothermic peak at 311 °C, which reflects the main thermal decomposition of chitosan. The decomposition of rifampicin occurs in three stages: the main stage begins at 195 °C to 260 °C with a mass loss of 16 %, the second stage proceeded smoothly in the range of 260–450 °C with a mass loss of 44 %, and the third stage (450–900 °C) resulted in a mass loss of 63 % (Figure 7*b*). The endothermic peak at 190 °C is accompanied by no mass loss, thus indicating the melting point of rifampicin. The exothermic peak at 255 °C is characteristic of the recrystallization process [3, 35]. CS-RIF nanoparticles demonstrate increased stability and similar mass loss pattern and thermal peaks (Figure 7*c*). At the same time, the thermal transitions characteristic of rifampicin is noticeably smoothed out, which may

indicate the transition of the substance to an amorphous state or its binding to the polymer matrix due to hydrogen bonding interactions [36].

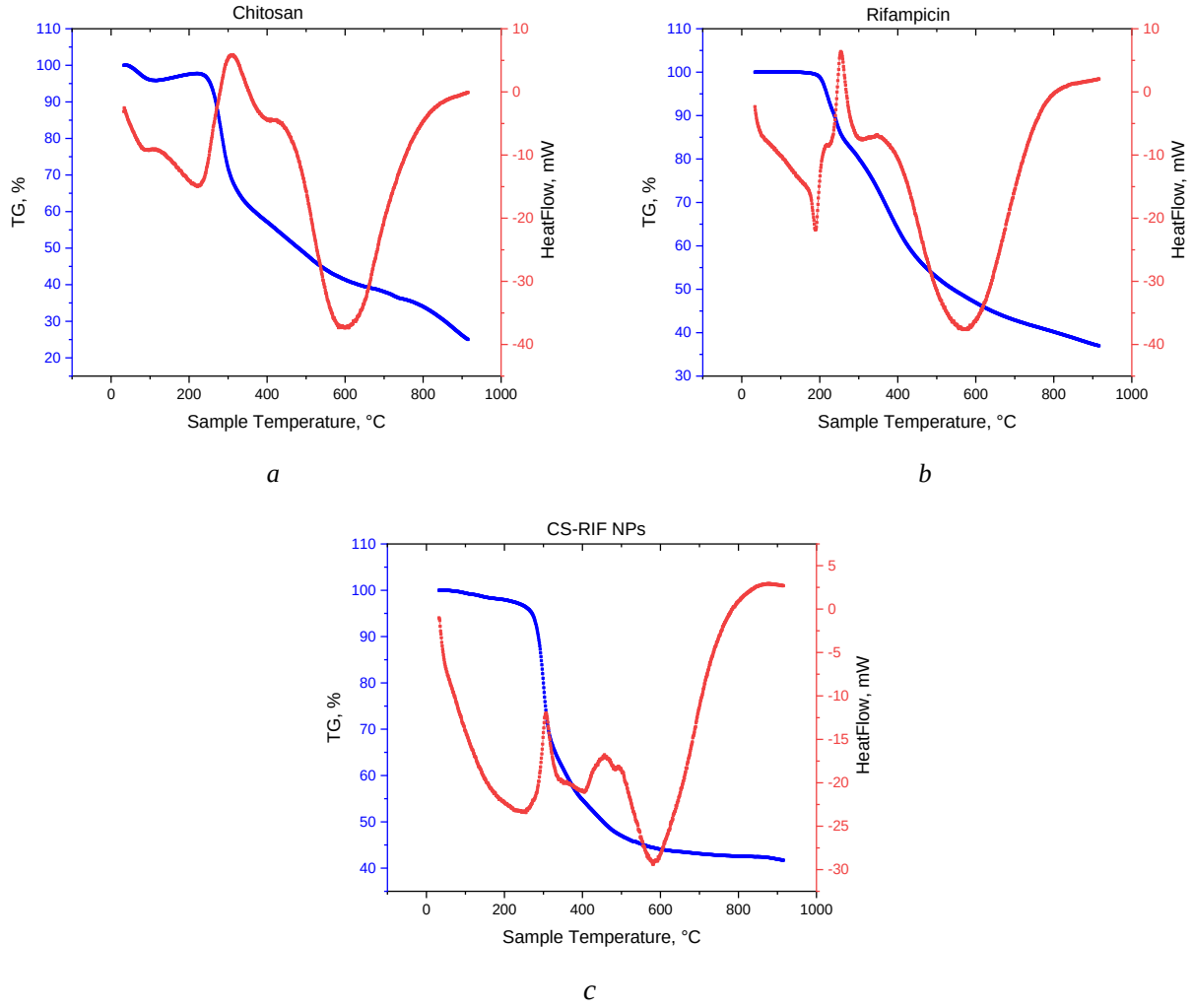

Figure 7. Thermal properties of the system components and the synthesized nanoparticles:
a — Chitosan; *b* — Rifampicin; *c* — CS-RIF nanoparticles

The FTIR technique was also used to determine the chemical composition and functional groups. FTIR spectra of rifampicin, chitosan nanoparticles without drug, and rifampicin loaded chitosan nanoparticles are shown in Figure 8. The chitosan samples show wide and intense absorption bands in the range of 3200–3600 cm^{-1}, which is explained by the overlapping stretching vibrations of –OH and $–NH_2$ characteristic of chitosan [37]. The bands at 2920 cm^{-1} correspond to C–H vibrations, at 1612 cm^{-1} to the C=O stretching of amide I, at 1543 cm^{-1} to the N–H bending and C–N stretching of amide II, at 1061 cm^{-1} to the C–N stretching of the amine, and at 1025 cm^{-1} to the skeletal C–O stretching vibrations [33, 37]. Rifampicin shows characteristic absorption bands at 3483 cm^{-1} associated with NH stretching, 1647 cm^{-1} corresponding to the C=O bond, 1458 cm^{-1} for the C=C bond, and 1381 cm^{-1} associated with CH_2 and C=C [31]. The low-frequency spectrum of CS-RIF nanoparticles shows characteristic peaks for chitosan and the rifampicin structure, indicating the absence of chemical interaction between the carrier and the drug.

Further research determined the *in vitro* rifampicin release kinetics from the chitosan-based nanoparticles matrix. To this end, the drug-loaded nanoparticles were studied using dialysis for 24 hours under conditions simulating the biological environment at different pH values (37 °C, pH 1.2; 6.8; 7.4). The rifampicin release profile is shown in Figure 9.

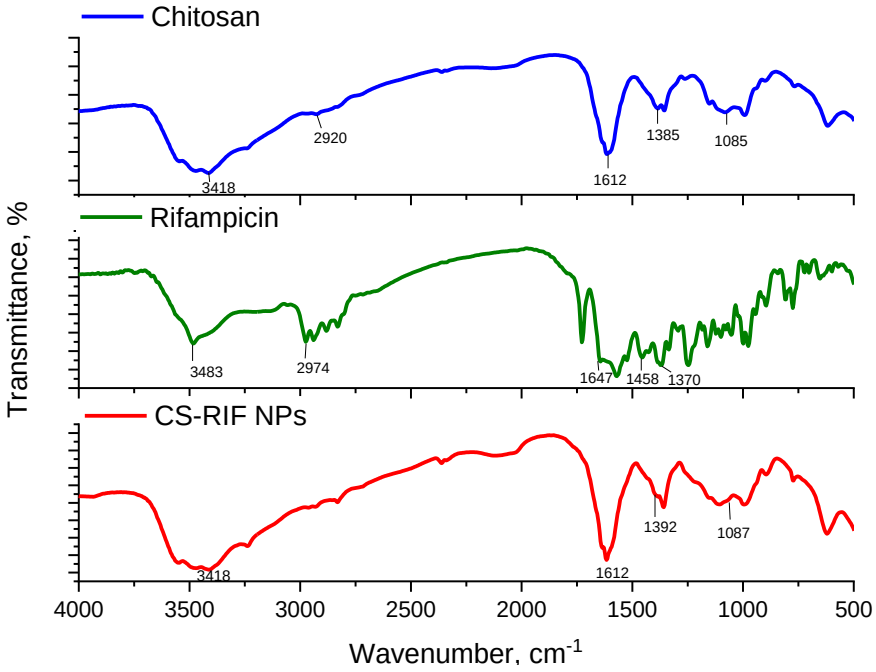

Figure 8. FTIR spectra for the rifampicin and the synthesized nanoparticles

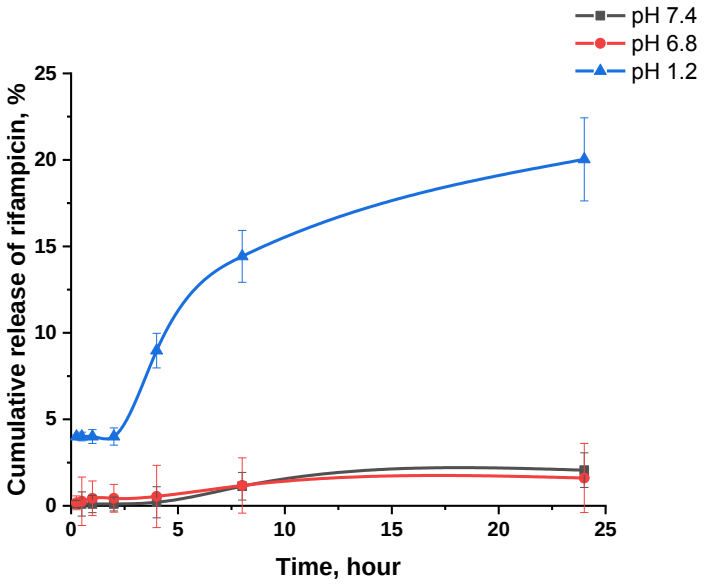

Figure 9. Cumulative release of rifampicin from CS-RIF nanoparticles under different pH conditions
(Values are shown as mean ± standard deviation (n = 3))

As can be seen from the graph, the kinetics of drug release significantly depend on the acidity of the medium. The most intense release is observed at pH 1.2, where the cumulative amount of released rifampicin reaches 20 % within 24 hours. In an acidic environment, partial protonation of the amino groups of chitosan occurs, which leads to an increase in solubility and swelling of the polymer matrix, facilitating the diffusion of the drug [38]. At pH 7.4 and 6.8, the release of rifampicin is significantly lower than 2 % in 24 hours. This can be explained by the limited solubility of chitosan in neutral and slightly alkaline conditions, in which the polymer network remains dense and less permeable to the diffusion of drug molecules [39]. Therefore, the obtained data confirm that the system based on chitosan nanoparticles has a pronounced pH dependence and is capable of providing controlled release of rifampicin.

Table 6 presents the results of a comparative analysis of mathematical models used to describe the kinetics of rifampicin release from chitosan nanoparticles at different pH values of 1.2, 6.8, and 7.4. Four models were evaluated: zero-order ($Q_t = Q_0 + k_0t$), first-order ($dC/dt = -kC$), Higuchi ($M_t/M_\infty = k\sqrt{t}$) and Korsmeyer–Peppas ($M_t/M_\infty = kt^n$) [40–42].

Table 6

Coefficients of determination (R^2) for rifampicin release models from CS-RIF nanoparticles

pH	Zero-order	First-order	Higuchi	**Korsmeyer–Peppas**
1.2	0.8827	0.8961	0.9452	0.8368
6.8	0.8815	0.8824	0.9541	0.9571
7.4	0.9408	0.9416	0.9183	0.6523

The highest correlation coefficient showed that rifampicin release follows Higuchi kinetics at pH 1.2. The release of rifampicin from chitosan nanoparticles at pH 7.4 showed a high correlation with the zero-order and first-order kinetic models, both with $R^2 > 0.94$. Rifampicin release at pH 6.8 is best described by the Higuchi model and the Korsmeyer-Peppas model ($R^2 > 0.95$). In the Korsmeyer-Peppas model for pH 1.2 and 6.8, the n coefficient values are below 0.5, indicating Fickian diffusion, while at pH 7.4, $n > 1$ and the release is based on a complex transport mechanism (super-random transport II) [41]. Thus, the data obtained confirm that the chitosan nanoparticle-based system has a pronounced pH dependence and is capable of providing controlled release of rifampicin.

The study of drug mucoadhesion is necessary to assess its effective retention on the mucous membrane for a long time. This is critical for the development of drug delivery systems to the lungs [43]. Incorporating RIF into chitosan nanoparticles can prolong the contact time of the drug with infected tissues. This is because chitosan is a mucoadhesive polymer that can interact with mucin present on the surface of mucous membranes through non-covalent interactions [44, 45]. Chitosan-based nanoparticles also demonstrate enhanced interaction with pulmonary mucus and alveolar macrophages [46–48]. In this regard, studies of the mucoadhesive properties of CS-RIF nanoparticles in acetate buffer solution (pH 5.5) and phosphate buffer solution (pH 6.8) were conducted, which made it possible to evaluate their behavior at two different pH levels. The pH value of 5.5 was selected to mimic the acidic environment of phagolysosomes in alveolar macrophages, while pH 6.8 represents near-physiological extracellular and mucosal conditions of the respiratory tract [49, 50]. The mucoadhesive properties of the nanoparticles were determined using the turbidimetric method over 4 hours. The results are shown in Figure 10.

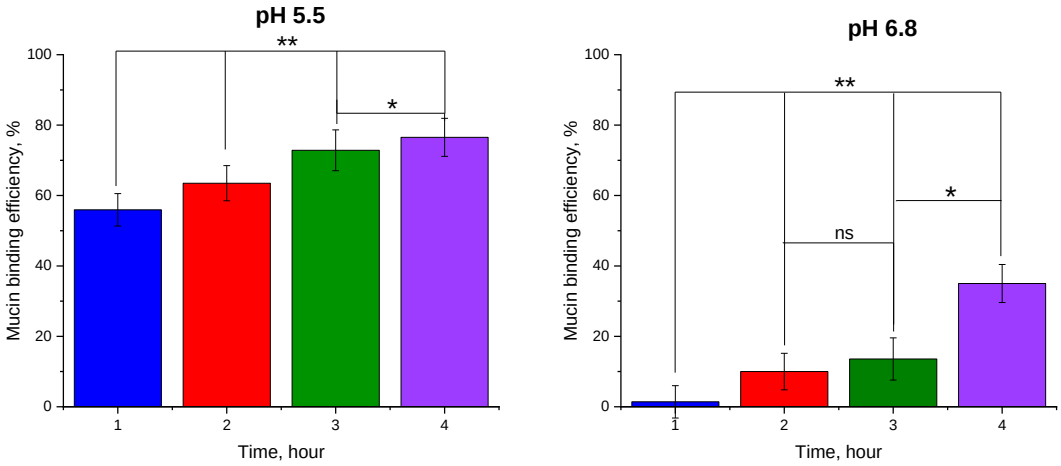

Figure 10. Mucin binding efficiency of CS-RIF nanoparticles with porcine mucin dispersions studied under different pH. "*" and "**" indicate $p < 0.01$ and < 0.005 respectively. ns — denotes no significant difference (Values are shown as mean ± standard deviation ($n = 3$))

As can be seen from the diagrams presented, the mucoadhesion of nanoparticles is better at pH 5.5. This is due to the good solubility of nanoparticles in the acetate buffer solution. Thus, in an acidic environment

(pH 5.5), it was 56 % after 1 hour and 77 % after 4 hours. When using a phosphate buffer solution with a pH of 6.8, the mucoadhesion of nanoparticles was 10 % after 2 hours and increased three times after 4 hours. These results highlighted the ability of chitosan nanoparticles to interact with the mucosa and maintain their adhesive potential across a wide range of physiological conditions, making the system promising for the delivery of rifampicin to the respiratory tract.

Conclusions

In this study, rifampicin-loaded chitosan nanoparticles were successfully prepared, optimized, and characterized. The optimized formula demonstrated nanoscale particle size, high loading efficiency, and controlled drug release profile, confirming the suitability of the developed system for prolonged-release rifampicin delivery. Mucosal adhesion studies at physiological pH values (5.5 and 6.8) showed that the nanoparticles have good adhesive properties and can be used for local delivery and prolonged retention on the mucosal surface. Overall, the results indicate the potential of chitosan-based nanoparticles as a delivery system for rifampicin. The developed system overcomes the significant drawbacks of traditional oral administration, which include low bioavailability and variability in drug concentration, and provides greater resistance to instability and release properties, as well as increased mucoadhesion. These results open up new opportunities for the development of improved inhalation drugs that can be used to reach the desired destination in the lungs and alveolar macrophages, leading to more effective and patient-friendly solutions for the treatment of tuberculosis.

Funding

This research was funded by the Science Committee of the Ministry of Science and Higher Education of the Republic of Kazakhstan under Grant No. AP23484897, titled “Creation of nanocarriers of antituberculosis drugs based on polysaccharide derivatives and their complexes”.

*Author Information**

**The authors' names are presented in the following order: First Name, Middle Name and Last Name*

Yerkeblan Muratovich Tazhbayev — Professor, Doctor of Chemical Sciences, Karaganda National Research University named after Academician E.A. Buketov, Universitetskaya street, 28, 100024, Karaganda, Kazakhstan; e-mail: tazhbaev@mail.ru; https://orcid.org/0000-0003-4828-2521

Aldana Rymzhanovna Galiyeva (*corresponding author*) — Leading researcher of the “Institute of chemical problems”, Karaganda National Research University named after Academician E.A. Buketov, Universitetskaya street, 28, 100024, Karaganda, Kazakhstan; e-mail: aldana_karaganda@mail.ru; https://orcid.org/0000-0002-8551-6297

Ulpan Yerlanqyzy Syrymova — Engineer, Karaganda National Research University named after Academician E.A. Buketov, Universitetskaya street, 28, 100024, Karaganda, Kazakhstan; e-mail: usyrymova@inbox.ru; https://orcid.org/0009-0007-8311-0414

Lyazzat Zhanybekovna Zhaparova — PhD, Associate Professor, Karaganda National Research University named after Academician E.A. Buketov, Universitetskaya street, 28, 100024, Karaganda, Kazakhstan; e-mail: lyazzh@mail.ru; https://orcid.org/0000-0003-1894-0255

Tolkyn Sergazyevna Zhumagaliyeva — Candidate of Chemical Sciences, Associate Professor, Karaganda National Research University named after Academician E.A. Buketov, Universitetskaya street, 28, 100028, Karaganda, Kazakhstan; e-mail: zhumagalieva79@mail.ru; https://orcid.org/0000-0003-1765-752X

Author Contributions

The manuscript was written through contributions of all authors. All authors have given approval to the final version of the manuscript. CRediT: **Yerkeblan Muratovich Tazhbayev** conceptualization, data curation, methodology, validation, visualization; **Aldana Rymzhanovna Galiyeva** data curation, visualization, formal analysis, writing-original draft; **Ulpan Yerlanqyzy Syrymova** investigation, formal analysis; **Tolkyn Sergazyevna Zhumagaliyeva** data curation, formal analysis; **Lyazzat Zhanybekovna Zhaparova** investigation, data curation, formal analysis.

Acknowledgments

Figure 1 and Graphical Abstract were created in *BioRender*. *Galiyeva, A. (2026) https://BioRender.com/ieb2gof*

Conflicts of Interest

The authors declare no conflict of interest.

References

1 World Health Organization (2025). Global tuberculosis report 2025. Geneva: World Health Organization. Retrieved from https://www.who.int/publications/i/item/9789240116924

2 Carnero Canales, C. S., Marquez Cazorla, J. I., Marquez Cazorla, R. M., Roque-Borda, C. A., Polinário, G., Figueroa Banda, R. A., Sábio, R. M., Chorilli, M., Santos, H. A., & Pavan, F. R. (2024). Breaking barriers: The potential of nanosystems in antituberculosis therapy. *Bioactive Materials*, 39, 106–134. https://doi.org/10.1016/j.bioactmat.2024.05.013

3 Yessentayeva, N. A., Galiyeva, A. R., Daribay, A. T., Sadyrbekov, D. T., Moustafine, R. I., & Tazhbayev, Y. M. (2024). Optimization of Polylactide-Co-Glycolide-Rifampicin Nanoparticle Synthesis, In Vitro Study of Mucoadhesion and Drug Release. *Polymers, 16*(17), 2466. https://doi.org/10.3390/polym16172466

4 Galiyeva, A. R., Tazhbayev, Ye. M., Zhumagaliyeva, T. S., & Daribay, A. T. (2022). Encapsulation of Isoniazid in Polylactide-Co-Glycolide Nanoparticles by Nanoprecipitation. *Bulletin of the University of Karaganda — Chemistry, 107*(3), 208–217. https://doi.org/10.31489/2022Ch3/3-22-17

5 Galiyeva, A. R., Tazhbayev, Ye. M., Zhumagaliyeva, T. S., Sadyrbekov, D. T., Kaikenov, D. A., Karimova, B. N., & Shokenova, S. S. (2022). Polylactide-co-glycolide nanoparticles immobilized with isoniazid: optimization using the experimental Taguchi method. *Bulletin of the Karaganda University. Chemistry Series, 105*(1), 69–77. https://doi.org/10.31489/2022ch1/69-77

6 Galiyeva, A. R., Tazhbayev, Y. M., Yessentayeva, N. A., Daribay, A. T., Marsel, D. T., Sadyrbekov, D. T., Zhaparova, L. Zh., & Arystanova, Z. T. (2023). PEGylation of Albumin Nanoparticles Immobilized with the Anti-Tuberculosis Drug "Isoniazid." *Eurasian Journal of Chemistry, 28*(2(110)). https://doi.org/10.31489/2959-0663/2-23-7

7 Sogias, I. A., Williams, A. C., & Khutoryanskiy, V. V. (2008). Why is Chitosan Mucoadhesive? *Biomacromolecules, 9*(7), 1837–1842. https://doi.org/10.1021/bm800276d

8 Žigrayová, D., Mikušová, V., & Mikuš, P. (2024). Advances in Chitosan Derivatives: Preparation, Properties and Applications in Pharmacy and Medicine. *Gels, 10*(11), 701. https://doi.org/10.3390/gels10110701

9 Morin-Crini, N., Lichtfouse, E., Torri, G., & Crini, G. (2019). Fundamentals and Applications of Chitosan. *Sustainable Agriculture Reviews 35*, 49–123. https://doi.org/10.1007/978-3-030-16538-3_2

10 Saputra, H. A., & Andreas. (2025). Chitosan and its biomedical applications: A review. *Next Materials*, 9, 101270. https://doi.org/10.1016/j.nxmate.2025.101270

11 Herdiana, Y., Febrina, E., Nurhasanah, S., Gozali, D., Elamin, K. M., & Wathoni, N. (2024). Drug Loading in Chitosan-Based Nanoparticles. *Pharmaceutics, 16*(8), 1043. https://doi.org/10.3390/pharmaceutics16081043

12 Jafernik, K., Ładniak, A., Blicharska, E., Czarnek, K., Ekiert, H., Wiącek, A. E., & Szopa, A. (2023). Chitosan-Based Nanoparticles as Effective Drug Delivery Systems—A review. *Molecules, 28*(4), 1963. https://doi.org/10.3390/molecules28041963

13 Grewal, A. K., & Salar, R. K. (2024). Chitosan nanoparticle delivery systems: An effective approach to enhancing efficacy and safety of anticancer drugs. *Nano TransMed*, 3, 100040. https://doi.org/10.1016/j.ntm.2024.100040

14 Dago-Serry, Y., Maroulas, K. N., Tolkou, A. K., Kokkinos, N. C., & Kyzas, G. Z. (2024). How the chitosan structure can affect the adsorption of pharmaceuticals from wastewaters: An overview. *Carbohydrate Polymer Technologies and Applications*, 7, 100466. https://doi.org/10.1016/j.carpta.2024.100466

15 Gonciarz, W., Balcerczak, E., Brzeziński, M., Jeleń, A., Pietrzyk-Brzezińska, A. J., Narayanan, V. H. B., & Chmiela, M. (2025). Chitosan-based formulations for therapeutic applications. A recent overview. *Journal of Biomedical Science, 32*(1). https://doi.org/10.1186/s12929-025-01161-7

16 Yang, C., Gao, S., Dagnæs-Hansen, F., Jakobsen, M., & Kjems, J. (2017). Impact of PEG Chain Length on the Physical Properties and Bioactivity of PEGylated Chitosan/siRNA Nanoparticles in Vitro and in Vivo. *ACS Applied Materials & Interfaces, 9*(14), 12203–12216. https://doi.org/10.1021/acsami.6b16556

17 Picchi, V., Gobbi, S., Fattizzo, M., Zefelippo, M., & Faoro, F. (2021). Chitosan Nanoparticles Loaded with N-Acetyl Cysteine to Mitigate Ozone and Other Possible Oxidative Stresses in Durum Wheat. *Plants, 10*(4), 691. https://doi.org/10.3390/plants10040691

18 Rampino, A., Borgogna, M., Blasi, P., Bellich, B., & Cesàro, A. (2013). Chitosan nanoparticles: Preparation, size evolution and stability. *International Journal of Pharmaceutics, 455*(1–2), 219–228. https://doi.org/10.1016/j.ijpharm.2013.07.034

19 Samprasit, W., Opanasopit, P., & Chamsai, B. (2021). Alpha-mangostin and resveratrol, dual-drugs-loaded mucoadhesive thiolated chitosan-based nanoparticles for synergistic activity against colon cancer cells. *Journal of Biomedical Materials Research Part B: Applied Biomaterials, 110*(6), 1221–1233. Portico. https://doi.org/10.1002/jbm.b.34992

20 Vieira, A. C. C., Chaves, L. L., Pinheiro, M., Lima, S. C., Neto, P. J. R., Ferreira, D., Sarmento, B., & Reis, S. (2021). Lipid nanoparticles coated with chitosan using a one-step association method to target rifampicin to alveolar macrophages. *Carbohydrate Polymers*, 252, 116978. https://doi.org/10.1016/j.carbpol.2020.116978

21 Vieira, A. C. C., Chaves, L. L., Pinheiro, S., Pinto, S., Pinheiro, M., Lima, S. C., Ferreira, D., Sarmento, B., & Reis, S. (2018). Mucoadhesive chitosan-coated solid lipid nanoparticles for better management of tuberculosis. *International Journal of Pharmaceutics*, *536*(1), 478–485. https://doi.org/10.1016/j.ijpharm.2017.11.071

22 Yanat, M., & Schroën, K. (2021). Preparation methods and applications of chitosan nanoparticles; with an outlook toward reinforcement of biodegradable packaging. *Reactive and Functional Polymers*, 161, 104849. https://doi.org/10.1016/j.reactfunctpolym.2021.104849

23 Jha, R., & Mayanovic, R. A. (2023). A Review of the Preparation, Characterization, and Applications of Chitosan Nanoparticles in Nanomedicine. *Nanomaterials*, *13*(8), 1302. https://doi.org/10.3390/nano13081302

24 Divya, K., & Jisha, M. S. (2017). Chitosan nanoparticles preparation and applications. *Environmental Chemistry Letters*, *16*(1), 101–112. https://doi.org/10.1007/s10311-017-0670-y

25 Rawal, T., Parmar, R., Tyagi, R. K., & Butani, S. (2017). Rifampicin loaded chitosan nanoparticle dry powder presents an improved therapeutic approach for alveolar tuberculosis. *Colloids and Surfaces B: Biointerfaces*, 154, 321–330. https://doi.org/10.1016/j.colsurfb.2017.03.044

26 Patel, B. K., Parikh, R. H., & Aboti, P. S. (2013). Development of Oral Sustained Release Rifampicin Loaded Chitosan Nanoparticles by Design of Experiment. *Journal of Drug Delivery*, 2013, 1–10. https://doi.org/10.1155/2013/370938

27 Fan, W., Yan, W., Xu, Z., & Ni, H. (2012). Formation mechanism of monodisperse, low molecular weight chitosan nanoparticles by ionic gelation technique. *Colloids and Surfaces B: Biointerfaces*, 90, 21–27. https://doi.org/10.1016/j.colsurfb.2011.09.042

28 Schnell, C. N., Galván, M. V., Solier, Y. N., Inalbon, M. C., Zanuttini, M. A., & Mocchiutti, P. (2021). High strength biobased films prepared from xylan/chitosan polyelectrolyte complexes in the presence of ethanol. *Carbohydrate Polymers*, 273, 118602. https://doi.org/10.1016/j.carbpol.2021.118602

29 Shilova, S. V., Tret'yakova, A. Ya., & Barabanov, V. P. (2018). Association of Chitosan in Aqueous-Alcohol Solutions. Polymer Science, Series A, 60(2), 184–189. https://doi.org/10.1134/s0965545x1802013x

30 Peyrovedin, H., Sajadian, S. A., Bahmanzade, S., Zomorodian, K., & Khorram, M. (2025). Studying the rifampin solubility in supercritical CO_2 with/without co-solvent: Experimental data, modeling and machine learning approach. *The Journal of Supercritical Fluids*, 218, 106510. https://doi.org/10.1016/j.supflu.2024.106510

31 Galiyeva, A., Daribay, A., Zhumagaliyeva, T., Zhaparova, L., Sadyrbekov, D., & Tazhbayev, Y. (2023). Human Serum Albumin Nanoparticles: Synthesis, Optimization and Immobilization with Antituberculosis Drugs. *Polymers*, *15*(13), 2774. https://doi.org/10.3390/polym15132774

32 Jogaiah, S., Mujtaba, A. G., Mujtaba, M., Archana, De Britto, S., Geetha, N., Belorkar, S. A., & Shetty, H. S. (2025). Chitosan-metal and metal oxide nanocomposites for active and intelligent food packaging; a comprehensive review of emerging trends and associated challenges. *Carbohydrate Polymers*, 357, 123459. https://doi.org/10.1016/j.carbpol.2025.123459

33 Alehosseini, E., Shahiri Tabarestani, H., Kharazmi, M. S., & Jafari, S. M. (2022). Physicochemical, Thermal, and Morphological Properties of Chitosan Nanoparticles Produced by Ionic Gelation. *Foods*, *11*(23), 3841. https://doi.org/10.3390/foods11233841

34 Onugwu, A. L., Attama, A. A., Nnamani, P. O., Onugwu, S. O., Onuigbo, E. B., & Khutoryanskiy, V. V. (2022). Development and optimization of solid lipid nanoparticles coated with chitosan and poly(2-ethyl-2-oxazoline) for ocular drug delivery of ciprofloxacin. *Journal of Drug Delivery Science and Technology*, 74, 103527. https://doi.org/10.1016/j.jddst.2022.103527

35 Alves, R., Reis, T. V. da S., Silva, L. C. C. da, Storpírtis, S., Mercuri, L. P., & Matos, J. do R. (2010). Thermal behavior and decomposition kinetics of rifampicin polymorphs under isothermal and non-isothermal conditions. *Brazilian Journal of Pharmaceutical Sciences*, *46*(2), 343–351. https://doi.org/10.1590/s1984-82502010000200022

36 Motiei, M., Pleno de Gouveia, L., Šopík, T., Vícha, R., Škoda, D., Císař, J., Khalili, R., Domincová Bergerová, E., Münster, L., Fei, H., Sedlařík, V., & Sáha, P. (2021). Nanoparticle-Based Rifampicin Delivery System Development. *Molecules*, *26*(7), 2067. https://doi.org/10.3390/molecules26072067

37 Kgoete, M. S., Mokgohloa, C. P., & Macevele, L. E. (2025). Synthesis of Chitosan Nanocomposite Materials Grafted with MWCNTs for the Removal of Tetracycline Pharmaceutical from Water Samples. *Colloids and Interfaces*, *9*(5), 69. https://doi.org/10.3390/colloids9050069

38 Herdiana, Y., Wathoni, N., Shamsuddin, S., & Muchtaridi, M. (2022). Drug release study of the chitosan-based nanoparticles. *Heliyon*, *8*(1), e08674. https://doi.org/10.1016/j.heliyon.2021.e08674

39 Ghosh, R., Mondal, S., Mukherjee, D., Adhikari, A., Ahmed, S. A., Alsantali, R. I., Khder, A. S., Altass, H. M., Moussa, Z., Das, R., Bhattacharyya, M., & Pal, S. K. (2022). Oral drug delivery using a polymeric nanocarrier: chitosan nanoparticles in the delivery of rifampicin. *Materials Advances*, *3*(11), 4622–4628. https://doi.org/10.1039/d2ma00295g

40 England, C. G., Miller, M. C., Kuttan, A., Trent, J. O., & Frieboes, H. B. (2015). Release kinetics of paclitaxel and cisplatin from two and three layered gold nanoparticles. *European Journal of Pharmaceutics and Biopharmaceutics*, 92, 120–129. https://doi.org/10.1016/j.ejpb.2015.02.017

41 Pavaloiu, R.-D., Sha'at, F., Hlevca, C., Sha'at, M., Savoiu, G., & Osman, S. (2021). Evaluation of drug release kinetics from polymeric nanoparticles loaded with poorly water-soluble APIs. *Ovidius University Annals of Chemistry*, *32*(2), 132–136. https://doi.org/10.2478/auoc-2021-0020

42 Jahangiri, S., Amirkhani, L., Akbarzadeh, A., & Hajimohammadi, R. (2023). Study of the Release Kinetic and the Diffusion Coefficient of Doxorubicin-Chrysin Coated with Fe_3O_4 and Polycaprolactone-Polyethylene glycol Copolymers. *Iranian Journal of Chemistry and Chemical Engineering*, *42*(5), 1436–1446.

43 Khutoryanskiy, V. V. (2018). Beyond PEGylation: Alternative surface-modification of nanoparticles with mucus-inert biomaterials. *Advanced Drug Delivery Reviews*, 124, 140–149. https://doi.org/10.1016/j.addr.2017.07.015

44 Kaldybekov, D. B., Shatabayeva, E. O., Polatkhan, A. A., Tuleyeva, R. N., Irmukhametova, G. S., & Khutoryanskiy, V. V. (2024). Development and Investigation of Mucoadhesive Polymers Based on Chitosan for Intravesical Therapy. *Eurasian Journal of Chemistry*, *29*(4(116)), 13–21. https://doi.org/10.31489/2959-0663/4-24-2

45 Phuong Ta, L., Bujna, E., Kun, S., Charalampopoulos, D., & Khutoryanskiy, V. V. (2021). Electrosprayed mucoadhesive alginate-chitosan microcapsules for gastrointestinal delivery of probiotics. *International Journal of Pharmaceutics*, 597, 120342. https://doi.org/10.1016/j.ijpharm.2021.120342

46 Tousian, B., & Khosravi, A. R. (2023). Chitosan-based pulmonary particulate systems for anticancer and antiviral drug carriers: A promising delivery for COVID-19 vaccines. *Results in Chemistry*, 6, 101146. https://doi.org/10.1016/j.rechem.2023.101146

47 Zacaron, T. M., Silva, M. L. S. e, Costa, M. P., Silva, D. M. e, Silva, A. C., Apolônio, A. C. M., Fabri, R. L., Pittella, F., Rocha, H. V. A., & Tavares, G. D. (2023). Advancements in Chitosan-Based Nanoparticles for Pulmonary Drug Delivery. *Polymers*, *15*(18), 3849. https://doi.org/10.3390/polym15183849

48 Rasul, R. M., Tamilarasi Muniandy, M., Zakaria, Z., Shah, K., Chee, C. F., Dabbagh, A., Rahman, N. A., & Wong, T. W. (2020). A review on chitosan and its development as pulmonary particulate anti-infective and anti-cancer drug carriers. *Carbohydrate Polymers*, 250, 116800. https://doi.org/10.1016/j.carbpol.2020.116800

49 Vandal, O. H., Nathan, C. F., & Ehrt, S. (2009). Acid Resistance in Mycobacterium tuberculosis. *Journal of Bacteriology*, *191*(15), 4714–4721. https://doi.org/10.1128/jb.00305-09

50 Nyberg, K., Johansson, U., Rundquist, I., & Camner, P. (1989). Estimation of pH in Individual Alveolar Macrophage Phagolysosomes. *Experimental Lung Research*, *15*(4), 499–510. https://doi.org/10.3109/01902148909069614